12-1991

Resonant Electron Transfer and K-Shell Excitation of Lithiumlike Projectiles in Collisions with Molecular Hydrogen

M. Anwar Kamal
Western Michigan University

RESONANT ELECTRON TRANSFER AND K-SHELL EXCITATION OF LITHIUMLIKE PROJECTILES IN COLLISIONS WITH MOLECULAR HYDROGEN

by

M. Anwar Kamal

A Thesis
Submitted to the
Faculty of The Graduate College
in partial fulfillment of the
requirements for the
Degree of Master of Arts
Department of Physics

Western Michigan University
Kalamazoo, Michigan
December 1991

RESONANT ELECTRON TRANSFER AND K-SHELL EXCITATION OF LITHIUMLIKE PROJECTILES IN COLLISIONS WITH MOLECULAR HYDROGEN

M. Anwar Kamal, M.A.

Western Michigan University, 1991

An experimental investigation of resonant transfer and excitation (RTE) for collisions of Mg^{9+} (lithiumlike) projectile ions with a molecular hydrogen gas target has been made. The experimental cross sections for projectile K-shell x rays coincident with electron capture in the energy of 33- to 60-MeV are found to be in good agreement with theoretical RTE calculations. The present results confirm the agreement between experiment and theory which has been reported for RTE involving K-shell excitation for projectiles with atomic numbers between 9 and 92 incident on H_2 and He targets.

Cross sections for total K-shell x-ray production and K-shell x rays coincident with electron loss as well as total single-electron-capture and total single-electron-loss were also measured for 33- to 60-MeV Mg^{9+} + H_2 collisions.

ACKNOWLEDGEMENTS

I would like to thank the faculty and staff of the Department of Physics of Western Michigan University, Kalamazoo for their direct or indirect contributions toward the realization of my thesis.

I wish to express special acknowledgement and sincere appreciation to Dr. Eugene M. Bernstein and Dr. John A. Tanis for their guidance, help, and encouragement for this thesis.

I also wish to thank Dr. Steve M. Ferguson for operating the tandem Van de Graaff accelerator on which this experiment was performed. I would like to thank Dr. Dean Halderson for reviewing this thesis and Dr. Roger Haar for assisting me with computer problems.

Finally, I wish to thank my wife, Naheed, for taking pain in typing this thesis; my daughter, Zill-e-Huma; and my son, Muneeb; for their love, support, and sacrifice needed for the completion of this thesis.

M. Anwar Kamal

Order Number 1346548

Resonant electron transfer and K-shell excitation of lithiumlike projectiles in collisions with molecular hydrogen

Kamal, Mohammed Anwar, M.A.

Western Michigan University, 1991

U·M·I
300 N. Zeeb Rd.
Ann Arbor, MI 48106

TABLE OF CONTENTS

LIST OF TABLES

LIST OF FIGURES

List of Figures--Continued

CHAPTER I

INTRODUCTION

When a fast incoming projectile ion collides with a neutral target atom, a number of well-known collision processes can take place. Some of these include the capture of one or more electrons from the target by the projectile (electron capture), ionization of one or more of the projectile electrons (electron loss), ionization of one or more of the target electrons, and excitation of either or both the projectile and target atom. Sometimes the reactants are left in excited states following the collision and photons or electrons may be emitted. The emitted electrons or photons may be independent of the collision or perturbed by it. Observation of the emitted radiation has led to much of our knowledge of the collision mechanism (Richard, 1975).

In an ion-atom collision, projectile excitation and charge transfer (capture) can take place together in a single encounter. This interaction produces a doubly excited intermediate state (Tanis et al., 1981). The doubly excited intermediate state can decay by either photon emission or electron emission (Auger decay). This process can be represented by the following:

$$A^{q+} + B \longrightarrow [A^{(q-1)+}]^{**} + B^{+}$$

$$[A^{(q-1)+}]^{**} \longrightarrow [A^{(q-1)+}]^{*} + h\upsilon \quad \text{(photon emission)}$$

$$[A^{(q-1)+}]^{**} \longrightarrow A^{q+} + e^{-} \quad \text{(electron emission)}$$

where A^{q+} is a fast projectile ion and B is a neutral target atom. The doubly excited intermediate state is represented by $[A^{(q-1)}]^{**}$.

Simultaneous capture and excitation in a single collision can be due to the electron-electron (correlated) interaction or through two electron-nucleus (uncorrelated) interactions (Tanis et al., 1985). In the electron-electron interaction a projectile electron interacts with a weakly-bound target electron in a manner analogous to the inverse of an Auger transition. In this interaction a resonant intermediate state is formed when the incident ion velocity relative to the target electron is equal to one of the projectile Auger-electron velocities. This process of correlated electron capture and projectile excitation with subsequent decay by photon emission is known as resonant-transfer-and-excitation (RTE) (Tanis et al., 1981). RTE is similar to dielectronic recombination (DR) (Seaton & Storey, 1976) except that for DR the captured electron is initially free whereas in RTE the captured electron is weakly bound. It should be noted that DR has been of

considerable interest in recent years since this mechanism finds application in the study of astrophysical plasmas (Burgess, 1964), in the development of nuclear fusion plasmas (Bitter et al., 1984), and in x-ray laser development (Whitten, Hazi, Chen, & Hagelstein, 1986). The fact that the target electron is not exactly free in RTE causes an energy broadening of the resonance due to the momentum distribution (Compton profile) of the target electrons (Brandt, 1983).

The uncorrelated mechanism involving electron excitation and capture is an interaction between the projectile nucleus and a target electron (electron capture) and between the target nucleus and a projectile electron (excitation). This is a two-step process for which the cross section increases sharply at low projectile ion energies and decreases exponentially as the energy is increased. This process is called nonresonant-transfer-and-excitation (NTE) (Pepmiller, 1983; Pempiller et al., 1985).

The main purpose of the present work was to investigate RTE for $Mg^{9+} + H_2$ collisions and to compare the experimental RTE cross sections with theoretical calculations. Previous measurements of RTE cross sections involving K-shell excitation for projectiles with atomic numbers from 14(Si) to 92(U) (Tanis, 1990 and references therein) were

found to be in reasonably good agreement with theory. However, K-shell RTE cross sections reported (Schulz et al., 1988) for $F^{6+} + H_2$ were about a factor of two smaller than the theoretical predictions (Bhalla & Karim, 1989; Badnell, 1990). Large differences between experiment and theory have also been found (Bernstein et al., 1989) for L-shell RTE in niobium ions. Since magnesium (Z=12) is between F(Z=9) and Si (Z=14) in the periodic table, it was felt worthwhile to ascertain whether or not measured K-shell RTE cross sections for Mg ions would agree with theory. It should be noted that recent measurements of K x-rays coincident with electron capture for $F^{6+} + H_2$ at Western Michigan University (Bernstein et al., 1991) are in agreement with RTE theory.

In the present work, lithiumlike Mg^{9+} ions with energies between 33 and 60 MeV were incident on a molecular hydrogen gas target. X-ray-particle coincidence techniques were used to investigate RTE involving K-shell excitation for this collision system. The experimental results are found to be in excellent agreement with theoretical RTE calculations (Badnell, 1990). Cross sections for single electron capture and single electron loss as well as cross sections for x rays coincident with one-electron loss were measured for the same collision system. The energy dependence of the electron capture

cross sections agrees well with an empirical scaling rule; however, the absolute values are about 35% larger than the predictions of the scaling rule.

CHAPTER II

THEORY

Resonant-Transfer-And-Excitation

Resonant-transfer-and-excitation (RTE) is a one-step recombination process analogous to dielectronic recombination (DR) as discussed in Chapter I. RTE and DR take place when capture of an electron is accompanied by simultaneous excitation of the ion resulting in the formation of a doubly-excited state. This excited state can decay to the ground state by photon emission or

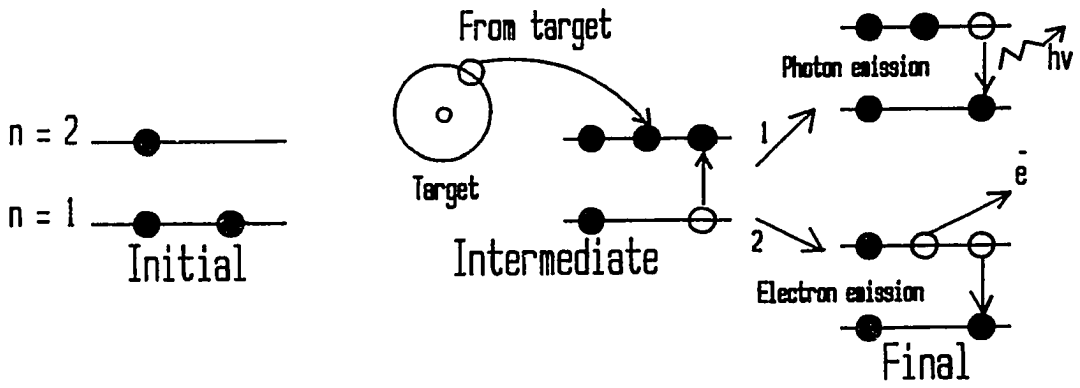

Figure 1. Schematic Diagram Showing the RTE or DR Process for a Lithiumlike Ion.

The intermediate doubly-excited state is formed via electron capture accompanied by simultaneous projectile excitation (Tanis, 1987).

electron emission as shown in Figure 1. By definition both RTE and DR can proceed through the photon decay mode.

RTE and DR take place only when the relative velocity between the incoming projectile ion and the captured electron matches the velocity of a possible Auger electron emitted from the projectile. Thus, the formation of the intermediate states proceeds via the inverse of an Auger transition, and the process is resonant. Many different electronic configurations are possible in the intermediate state as illustrated in Figure 2. An RTE or DR recombination event is designated as a KLL transition when a

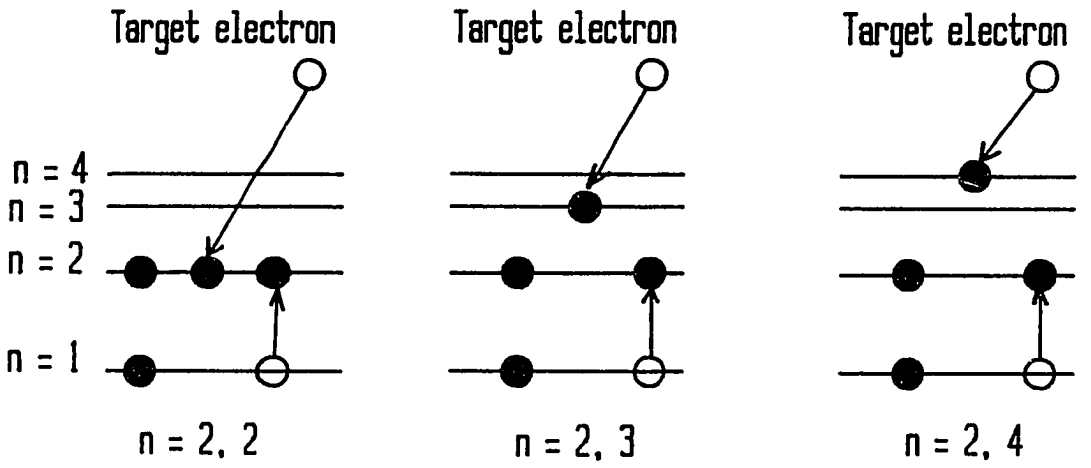

Figure 2. Schematic Diagram Showing Formation of Different Resonance States.

The formation of resonance states involves different principal quantum Numbers (n = 2,3; n = 2,4; etc) of the two active electrons (Tanis, 1987).

projectile K-shell electron is excited to the L-shell and the projectile captures a target electron into the L-shell. This type of event is labelled n = 2, 2 in Figure 2. A KLn (n > L) transition occurs when a projectile electron from the K-shell is excited to the L-shell and a target electron is captured into an M or higher shell (n = 2, ≥ 3 in Figure 2).

In the RTE process one is usually only interested in the projectile ion so no consideration is given to the target atom after it loses an electron in the event.

Furthermore, in RTE the projectile ion captures a weakly bound target electron, not a free electron as in DR. The target electron is characterized by its momentum distribution (Compton profile). Thus in the rest frame of the projectile, the electrons of a given target populate a range of energies. In this respect RTE is similar to radiative electron capture (REC) of a bound target electron into an inner shell of the projectile. Radiative electron capture (REC) is a process in which a projectile ion captures a free or weakly bound target electron directly into a K-shell vacancy with the subsequent emission of an x-ray photon (Schnopper et al., 1972). The energy of the photon is given approximately by the sum of the binding energy of a K-electron in a hydrogenlike or heliumlike ion and the kinetic energy of an electron which is at rest in

the target relative to the moving projectile ion. The difference is, however, that in REC the electron can be captured from a continuum state of any energy into a bound state of the projectile, the excess energy being taken away by photon emission (inverse of the photoelectric effect), whereas in RTE the energy of the initial continuum state has to match the energy of the intermediate resonance state (inverse of the Auger effect).

Brandt (1983) derived a theory relating RTE to DR using the impulse approximation. In this approximation it is assumed that after the collision the separation between the projectile and target is such that there is no further interaction and thus the distortion of projectile resonance state by the target nucleus is small. In order to satisfy this condition, the ion velocity should be much greater than the bound target electron velocity. The bound electrons are, thus, considered "quasi-free." The RTE cross-section for a given target atom is then derived by summing over the contributions of all the "quasi-free" target electrons, and is given by Brandt (1983) as

$$\sigma_{RTE}Total = \left(\frac{M}{2E}\right)^{1/2} \Delta\epsilon \, \bar{\sigma}_{DR} \sum_i J_i(P_{iz}) . \qquad (2.1)$$

Equation (2.1) represents the total RTE cross section involving formation of an intermediate state followed by x-ray emission, where M and E are the mass and energy of

the projectile ion, respectively. The average DR cross section, $\tilde{\sigma}_{DR}$, is averaged over the energy interval $\Delta\epsilon$, and $J_i(P_{iz})$ is the probability of finding a particular target electron with momentum component P_{iz} along the beam axis (direction of the incident beam). $J_i(P_{iz})$ is also known as the Compton profile (momentum distribution of the target electron).

As seen from equation (2.1) the RTE cross section depends directly on $J_i(P_{iz})$. Figure 3 shows the Compton profile of different neutral target atoms. Biggs, Mendelsohn and Mann (1975) calculated Compton profiles of different neutral target atoms using Hartee-Fock and relativistic Dirac-Hartee-Fock wave functions. Mathematically the Compton profile can be represented as

$$J_i(P_{iz}) = \int\int_{-\infty}^{+\infty} dP_{ix}dP_{iy}|\psi_i(P_i)|^2. \qquad (2.2)$$

Equation (2.2) represents a symmetric Gaussian function of momentum having a maximum value at P(momentum) = 0. As shown in Figure 3 the width depends on Z of the neutral atom and on the particular orbit. The RTE cross-section includes the total contributions of all the available weakly bound target electrons which can take part in the formation of the various intermediate resonance states.

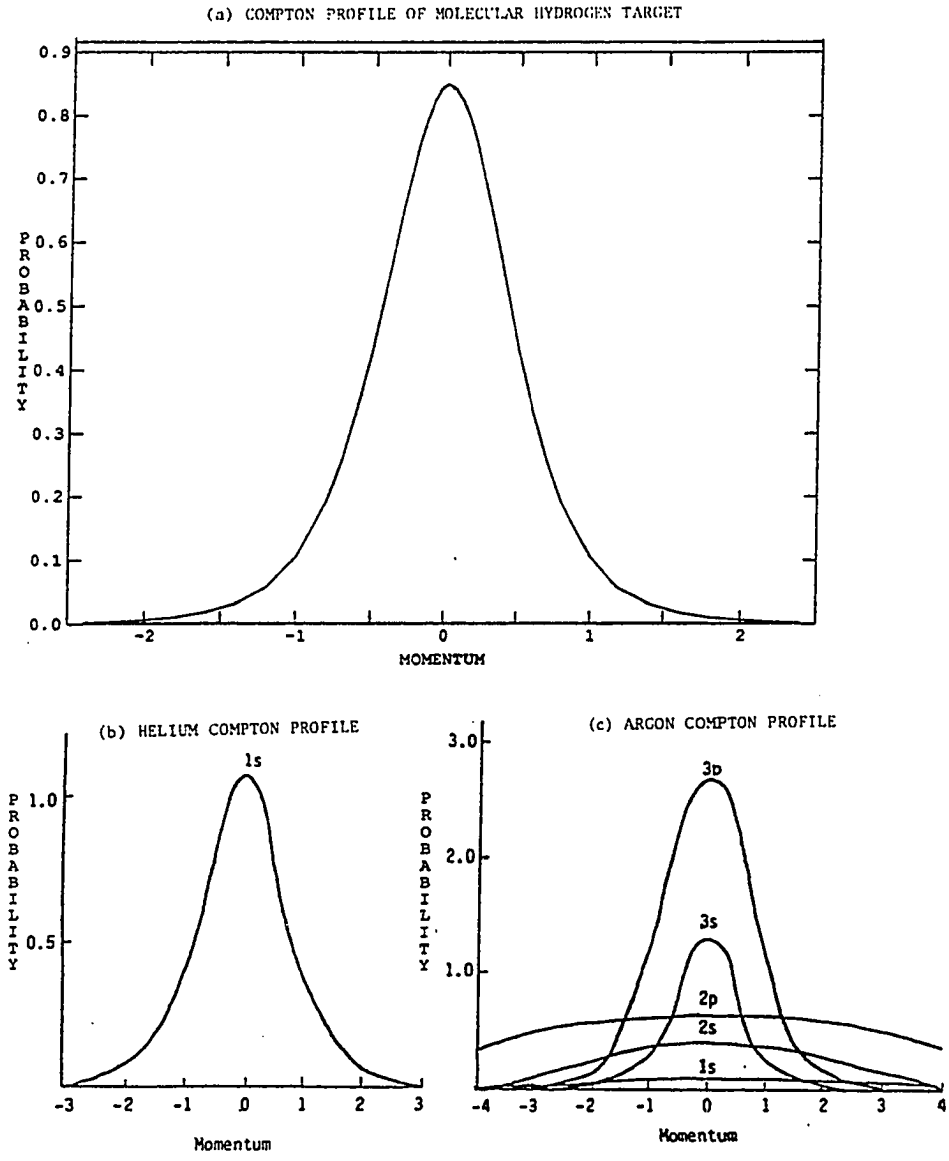

Figure 3. Hartee-Fock Compton Profiles of Individual Orbitals for Different Neutral Targets (Biggs, Mendelsohn, and Mann, 1975).

(a) Molecular Hydrogen, (b) Helium, and (c) Argon.

The overall profile of the RTE cross section curve depends on the positions and relative magnitudes of the DR resonances of the projectile and on the Compton profile of the target electrons. The width of the Compton profile varies with the velocity of the target electrons, and therefore on the atomic number of the target. The variation in magnitude of the individual DR peaks does not depend strongly on the atomic number of the projectile (Hahn, 1982).

General considerations of the RTE profiles expected for different projectile and target systems can be investigated qualitatively by considering the energy separation between individual resonance states in the projectile DR spectrum and the Compton profile of the target. The energy difference between the resonance states depends on the square of the atomic number of the projectile ion. If one has a broad Compton profile (heavy target) compared to the energy spacing between individual resonance states (or groups of states) in the DR spectrum, the RTE profile will have only one maximum as shown in Figure 4a. This occurs when a "light" ($Z_{projectile}/Z_{target} < 10$) projectile is incident on a heavy target, and individual resonance states, or groups of resonance states cannot be resolved. In the other case in which the Compton profile is narrow as compared to the energy spacing between the individual

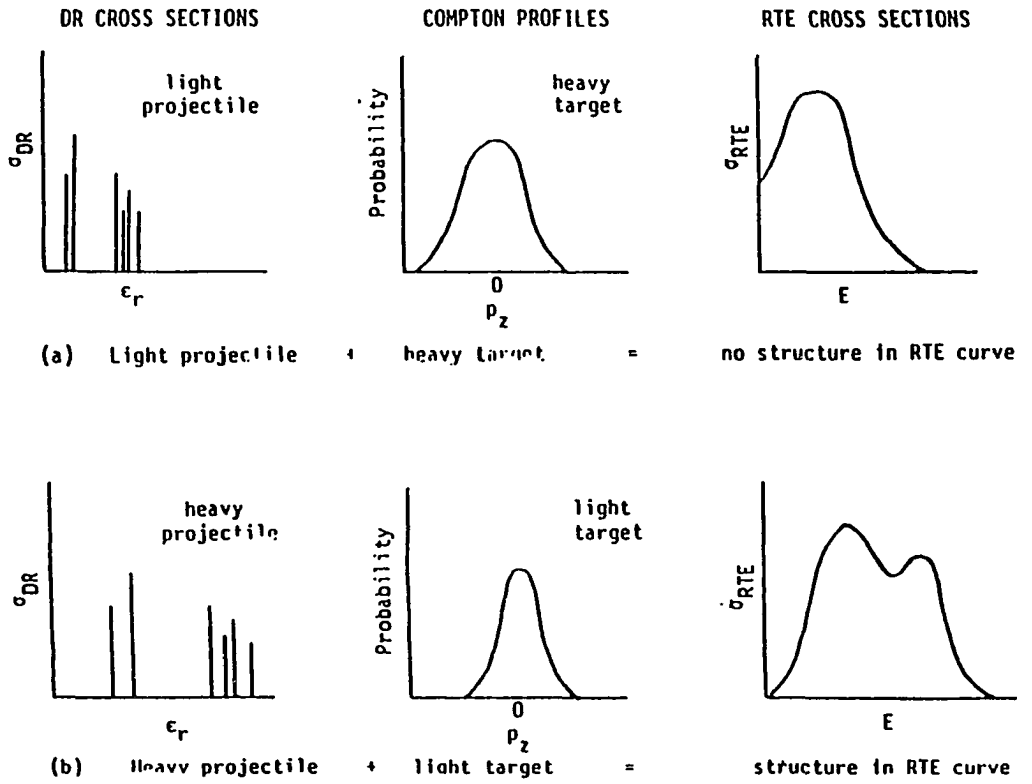

Figure 4. Qualitative Schematic Representation of Structure and No Structure Cases of RTE Cross Section Curves With Respect to the Projectile Ion and Neutral Target Atomic Weights (from Oglesby based on calculations by McLaughlin and Hahn, 1982 and Biggs, Mendelsohn and Mann, 1975).

resonance states (or groups of states) in the DR spectrum, the RTE profile may have more than one maximum. This corresponds to a "heavy" ($Z_{projectile}/Z_{target} > 10$) projectile incident upon a light target. This situation is shown in Figure 4b. The lower energy maximum produces K_α x rays only since both of the active electrons have principal quantum number $n = 2$ (see Figure 2). The higher energy maximum produces both K_α and K_β x rays since $n \geq 3$ for one of the active electrons. Experimentally one can often distinguish between K_α and K_β x-rays.

Until recently, DR cross-sections were very difficult to measure directly because such experiments require a high density target of free-electrons which is difficult to construct. DR measurements further require a very high vacuum since electrons can be readily captured in even very low background gas densities. Low particle density and inhomogeneity of the beams cause errors and uncertainties. Because of the low beam densities, there is another difficulty of long running times to collect a significant number of events. DR cross-sections have been measured using crossed (Belic, Dunn, Morgan, Mueller, & Timmer, 1983) and merged (Dittner et al., 1983; Mitchell et al., 1983) beam techniques, while recent measurements use the techniques of ion traps, electron coolers, and storage rings (Knapp et al., 1989; Andersen, Hvelplund, Knudsen, &

Kvistgaard, 1989; Ali, Bhalla, Cocke, & Stockli, 1990; Kilgus et al. 1990). These recent improved techniques of measurements have provided the first stringent tests of DR theory.

Several theoretical DR calculations have been carried out (McLaughlin & Hahn, 1982; Lagattuta & Hahn, 1983; Nasser & Hahn, 1983; Badnell, 1990). It was found that the theoretical results for RTE with L-shell excitation in Na-, Mg-, and Al-like Nb ions (Hahn et al., 1987; Badnell, 1990) vary considerably from the experimental (Bernstein et al., 1989) values.

Calculated DR cross sections for lithiumlike sulfur are shown in Figure 5 in which the different intermediate resonance states are indicated. The height of each line in Figure 5 represents the relative probability of the formation of that particular excited state as a result of simultaneous capture and excitation (i.e., DR).

A number of experimental and theoretical studies have clearly demonstrated that RTE closely approximates DR, and the close relationship between RTE and DR allows RTE to be used as a test of theoretical DR cross sections (Tanis, 1990). Except for the case of F^{6+} mentioned in Chapter I, previous studies have shown that the measured magnitude and peak energy locations for K-shell RTE cross sections are in reasonable agreement with calculations of RTE based on

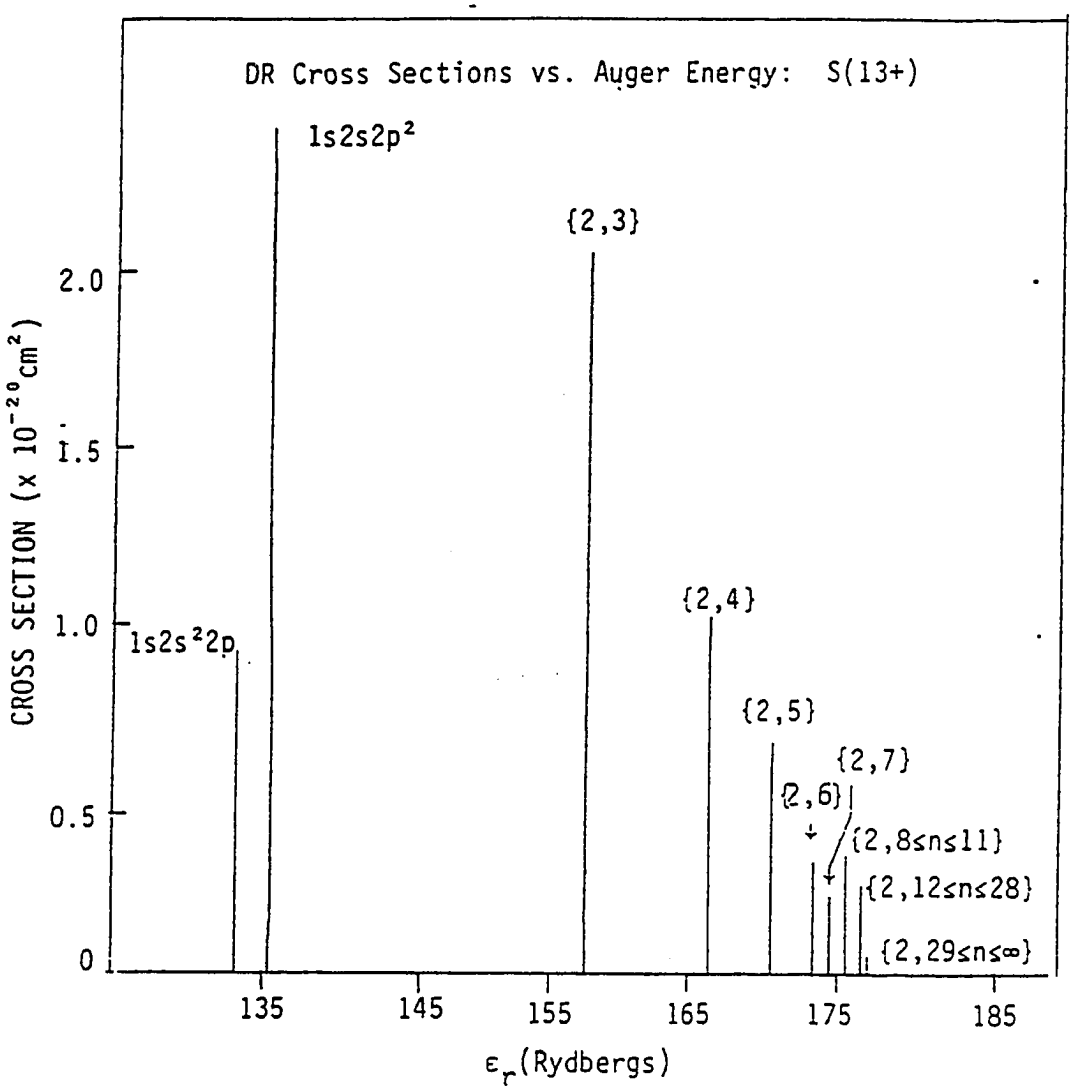

Figure 5. Positions and Intensities of Calculated Dielectronic Recombination Cross Sections for Lithium-like Sulfur, S^{13+}, Showing Different Resonance States.

The configurations of the various states are indicated (figure from McLaughlin and Hahn, 1982).

theoretical DR cross sections. The only extensive study for L-shell excitation (Bernstein et al., 1987, 1989) is for Nb^{q+} ions.

RTE contributes in a characteristic way to the projectile vacancy production in ion-atom collisions. The existence of RTE also demonstrates the importance of the electron-electron interaction in the dynamics of fast ion-atom collisions. The shape of the RTE feature reflects the momentum distribution of the target electrons, the position of the cross-section maximum is determined by the resonance energy, and its absolute magnitude is proportional to the DR cross section. Thus, the measurement of RTE cross-sections as a function of projectile energy allows one to test calculations of the resonance energies and DR cross sections for the projectile and the Compton profile for the target, under the conditions of the impulse approximation.

Total Electron Capture

Electron capture is a process of fundamental interest (Knudsen et al., 1981) and can be illustrated as

$$A^{q+} + B \rightarrow A^{(q-1)+} + B^{+}$$

where A^{q+}, an approaching projectile ion, interacts with a neutral gas target B and in the collision A^{q+} captures one electron from B and emerges as $A^{(q-1)+}$.

There has been a continuing interest in such process-

es, partly due to the fact that in single collisions between ions and atoms, the electron-capture exit channel is often associated with a large cross section (Knudsen et al., 1981). This makes the process important for the understanding of such collisions. Electron capture is also of interest because of the influence of charge exchange on the slowing down of atomic particles passing through matter (Knudsen et al., 1981).

In recent years there has been a substantial increase in the activity in this field as regards theoretical as well as experimental investigations (Knudsen et al., 1981; Schlachter et al., 1983). This renewed interest stems from the fact that electron-capture processes have been found to be crucial for the performance of thermonuclear-fusion devices (Drawin, 1978) as well as for a variety of other applications like accelerator design, beam transport, and fusion plasmas (Steigman, 1975). Drawin (1978) found such elementary reactions to be important when he investigated the dynamics of hydrogen, helium, and oxygen tokamak reactions and the products of their interactions. In general, electron capture (and loss) depend on the beam energy, projectile charge state, and target Z. Considering the vast number of combinations of projectile species, energies and charge states, and the large number of possible gas and vapor targets, scaling rules are useful.

Such rules can be used to predict the magnitude of unmeasured cross sections (Knudsen et al., 1981; Schlachter et al., 1983).

Knudsen et al. (1981) derived a scaling rule for single-electron capture based on the classical theory of Bohr and Lindhard (Bohr & Lindhard, 1954). Schlachter et al. (1983) derived an empirical scaling rule for single-electron capture. This latter rule was derived by fitting an empirical function to a number of experimental values of electron capture cross section measurements for a range of projectile energies, charge states, and target atomic number. Recently a revised scaling rule, valid for helium targets and based on measurements using several incident ions, was obtained (Schlachter et al., 1987).

The newer electron capture scaling rule (Schlachter et al., 1987) which will be compared with measurements made in the present experiment is given as follows:

$$\tilde{\sigma} = (1.1x10^{-8}[1-\exp(-0.037\tilde{E}^{2.2})] \\ x[1-\exp(-2.44)x10^{-5}\tilde{E}^{2.6})]/\tilde{E}^{4.8} \qquad (2.3)$$

where

$$\tilde{\sigma} = \sigma Z^{1.8}/q^{0.7} \qquad (2.4)$$

and

$$\tilde{E} = E/(Z^{1.25}q^{0.5}) .$$

The reduced cross section, $\tilde{\sigma}$, and the cross section, σ, are in units of cm^2/atom. The reduced energy, $\tilde{E}$, and the energy, E, are in units of keV/u. The incident projectile charge state is q, and Z is the atomic number of the target.

CHAPTER III

EXPERIMENTAL PROCEDURES

The present experiment was conducted at Western Michigan University, Kalamazoo using the 6 MV EN tandem Van de Graaff accelerator. A beam of 33-60 MeV Mg^{9+} (lithiumlike) ions from this accelerator was incident on an H_2 gas target. A general schematic of the accelerator is shown in Figure 6.

Magnesium ions were obtained from a source of negative ions produced by cesium sputtering (SNICS). Since magnesium has a negative electron affinity it does not form a metastable negative ion with a significant lifetime. Therefore, it was necessary to accelerate a molecule, MgH^-_2 or MgH^-_3, in the present experiment.

A carbon foil inside the accelerator terminal stripped off electrons and turned the negative magnesium ion molecules into positive ions which were further accelerated by the high positive terminal voltage. The ions from the accelerator were momentum analyzed by a 90° analyzing magnet and passed through a thin carbon post acceleration stripping foil (of thickness 5-20 $\mu g/cm^2$) to produce a distribution of charge states. The charge state of

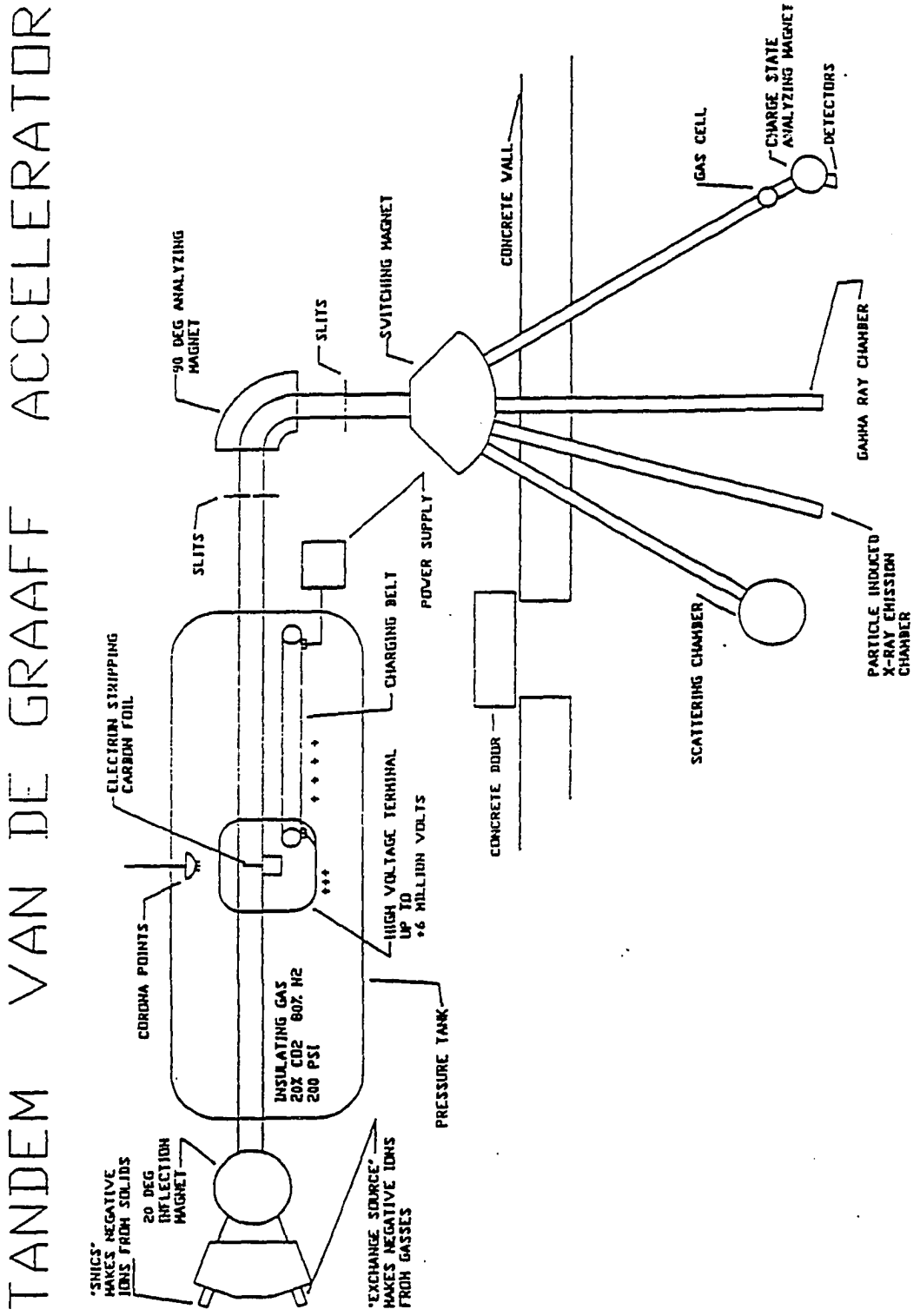

Figure 6. General Schematic of the WMU EN Tandem Van de Graaff Accelerator.

interest (9^+) was then selected by a switching magnet which directed the ions down the beam line to the target chamber. A schematic of the beam line used for this experiment is shown in Figure 7. The beam was collimated by two sets of square apertures about 1 mm x 1 mm located at approximately 225.0 cm and 75.0 cm in front of the target cell. The target chamber consisted of a differentially pumped gas cell defined by four optically aligned circular apertures. The inner set of apertures define the target length for the charge exchange measurements.

The pumping of the gas cell was accomplished by means of an oil diffusion pump connected to the gas cell. A schematic of the target region is shown in Figure 8. Two other diffusion pumps were also utilized to maintain a residual gas pressure of 10^{-6} to 10^{-7} torr in the beam line. A constant pressure was maintained in the target chamber by means of an automatic pressure controller. The pressure was monitored by a capacitance manometer. Each run was performed at a well-defined target gas cell pressure. For many energies, measurements were made for three different target pressures. In some cases measurements were made for pressures of 100 microns and zero microns only.

A 28.0 mm^2 Si(Li) detector with a 7.62 x 10^{-3} mm Be window was placed at an angle of 90° to the incoming projectile beam axis to detect the Mg K-shell x rays.

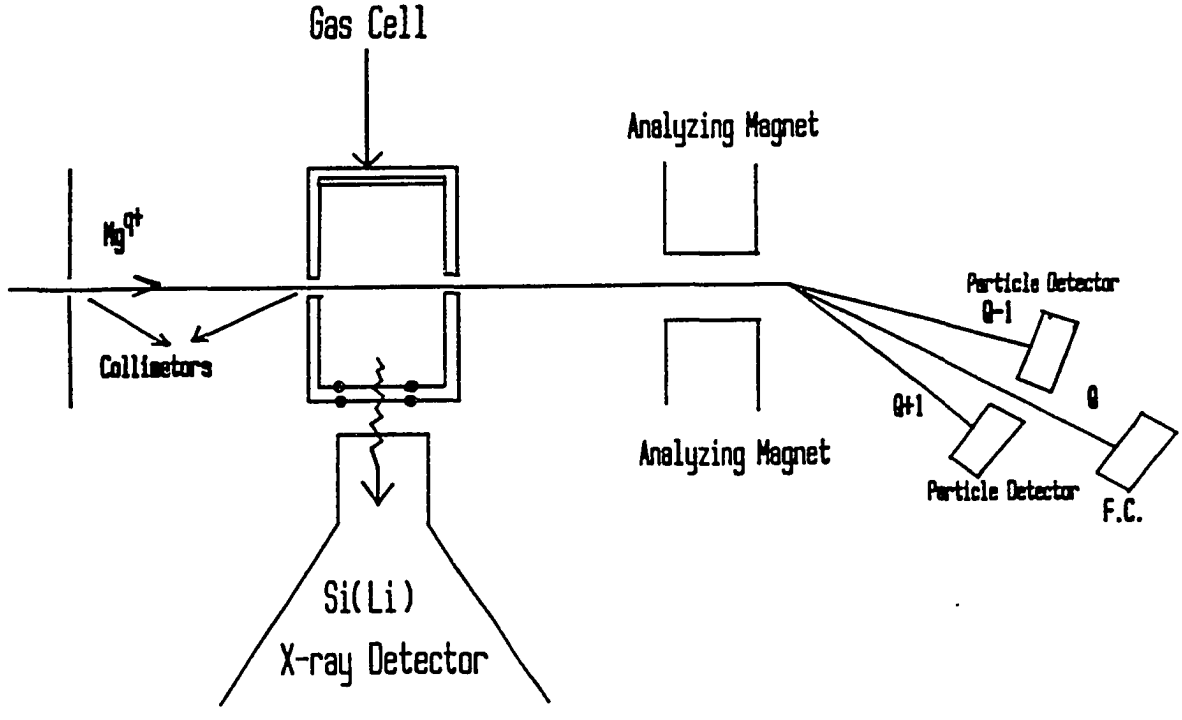

Figure 7. Schematic of the Atomic Physics Beam Line at WMU.

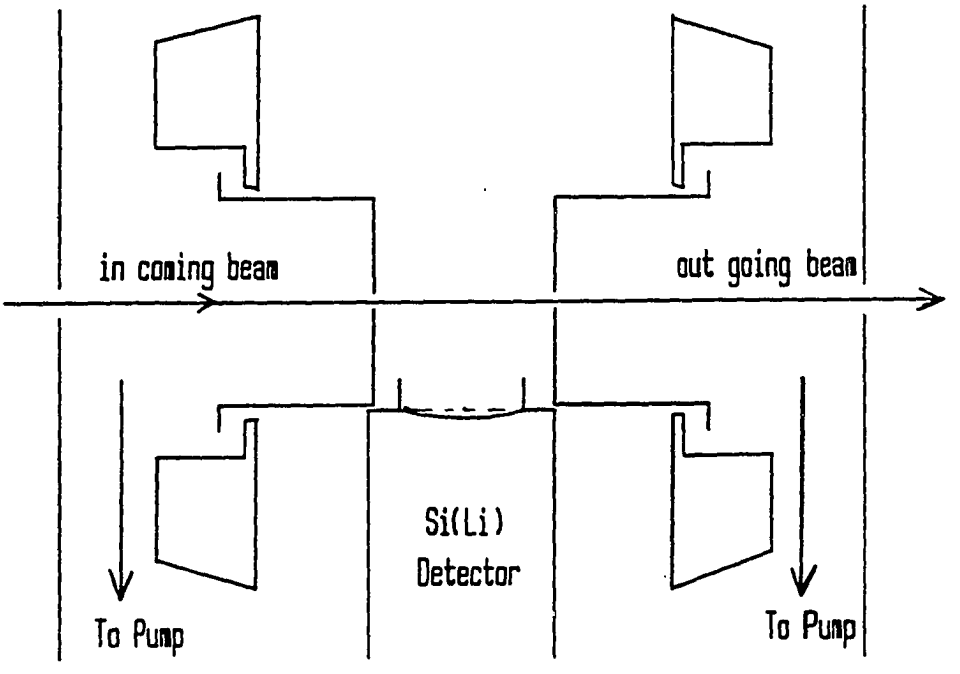

Figure 8. Schematic of the Target Region Consisting of a Differentially Pumped Gas Cell and Si(Li) Detector.

Because of the geometry of the x-ray detector, the effective target length seen by this detector is shorter than the target length for the charge exchange measurements.

Since the coincident count rate is limited by the maximum useable count rate in the particle detectors, a special set of apertures were used to minimize the difference in the effective target length for x-ray events compared to that for charge-change events. Because of these special apertures the effective target length for the charge-change events was not as well defined as in the normal arrangement. Thus, there is an increase in the uncertainty in the results for the electron capture and loss measurements.

Following the gas cell, an electromagnet was used (Figure 7) to spatially separate the various charge states of the outcoming beam. After separating the charge states, the charge-changed components were detected using surface barrier detectors supplied by EG & G ORTEC, Oak Ridge, Tennessee.

One detector was used to detect magnesium ions that had captured a target electron and a second detected ions that has lost an electron. The non-charge-changed beam was collected in a Faraday Cup, held at -300 volts to suppress the secondary electrons and the current was measured with a Keithley electrometer. The ratio of charge-changed ions

to the total number of incident particles is the fraction of the projectiles which have captured or lost an electron. The signature for an RTE event is the simultaneous capture of an electron and the emission of a Mg K x ray. Thus, coincidences between x rays and charge-changed ions were measured.

Figure 9 shows a schematic block diagram of the electronics used in the experiment. The coincidence events were recorded by ORTEC 566 time-to-amplitude-converters (TAC). The start signals for the TACs come from the Si(Li) x-ray detector viewing the gas cell whereas the stop signals originate from the surface barrier particle detectors. Start-to-stop time conversion is accomplished only after a valid start (x-ray pulses of a specified amplitude received from CFD) has been identified and after a stop pulse has arrived within the selected time range. The x-ray pulses received from the Si(Li) detector are routed through a timing filter amplifier (TFA) to obtain a fast timing signal. The output of the TFA is routed through a constant fraction discrimination (CFD) which accepts negative input pulses and converts the analog signal (which is proportional to the amplitude of the x-ray pulse) into a logic signal, provided the amplitude of the input signal is above the minimum setting of the discriminator. The output of the CFD, which is a logic signal, is

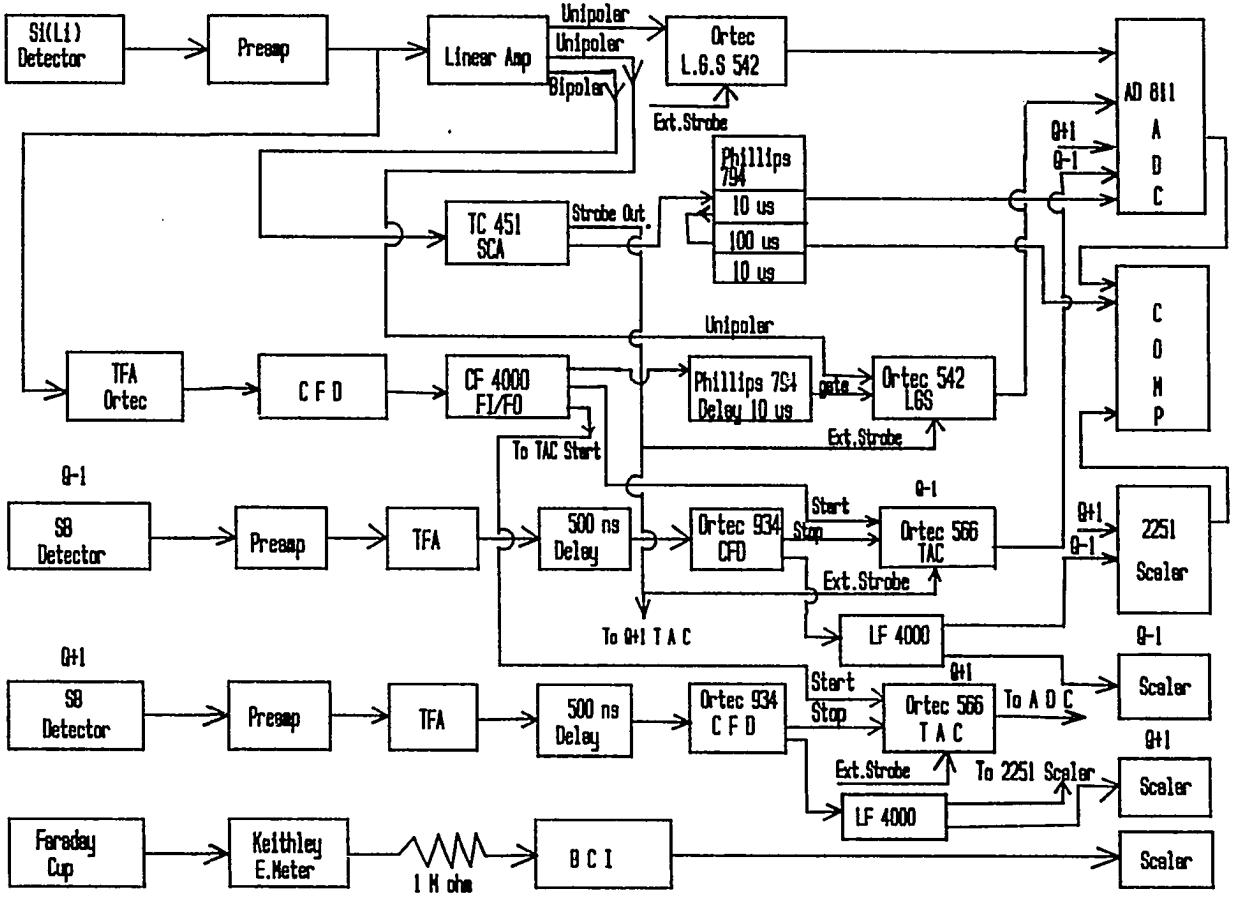

Figure 9. Block Diagram of the Electronics Used in the Measurement of Mg^{9+} + H_2 Collisions to Detect Charge-Changed Projectile Ions in Coincidence with K X-Rays.

used as the start signal for the time-to-amplitude converters.

The signals from charge-changed projectile ions striking the surface-barrier detectors (SB) were also routed through pre-amplifiers and timing-filter-amplifiers. These signals, however, were delayed by long cables (about 500 ns) before reaching constant-fraction-discriminators. The delay in the particle channel is adjusted to provide the necessary time difference between the start and stop signals. The TAC then outputs an analog pulse whose amplitude is proportional to the time difference between the start and stop signals. The x-ray and particle gates are closed after each TAC output until the next x-ray of sufficient energy is observed.

Measurements were carried out for single electron capture, (Q-1), and loss, (Q+1), the total K-shell x-ray emission, and coincidences between x-rays and electron capture and x rays and electron loss. Figure 10 shows a typical TAC spectrum for K-shell x rays coincident with electron capture. Also shown in Figure 10 is a total K x-ray spectrum. The x-ray and TAC spectra were analyzed by integrating the number of counts in each peak. The fraction of ions emerging in each charge state for a given pressure were calculated and the relative fractions were plotted as a function of target gas pressure. Figure 11

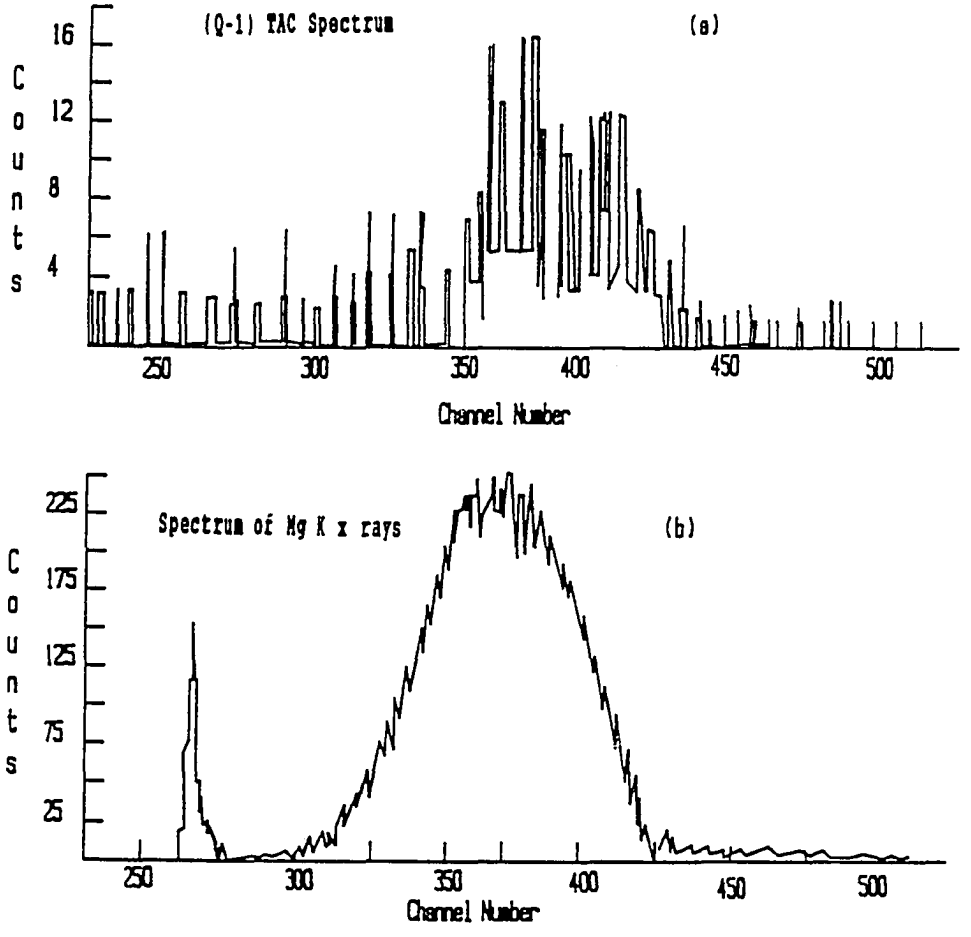

Figure 10. Plots of (a) TAC Spectrum for K X-Rays and Projectiles Which Captured an Electron (b) Total X-Ray Spectrum for Mg^{9+} + H_2 Collisions.

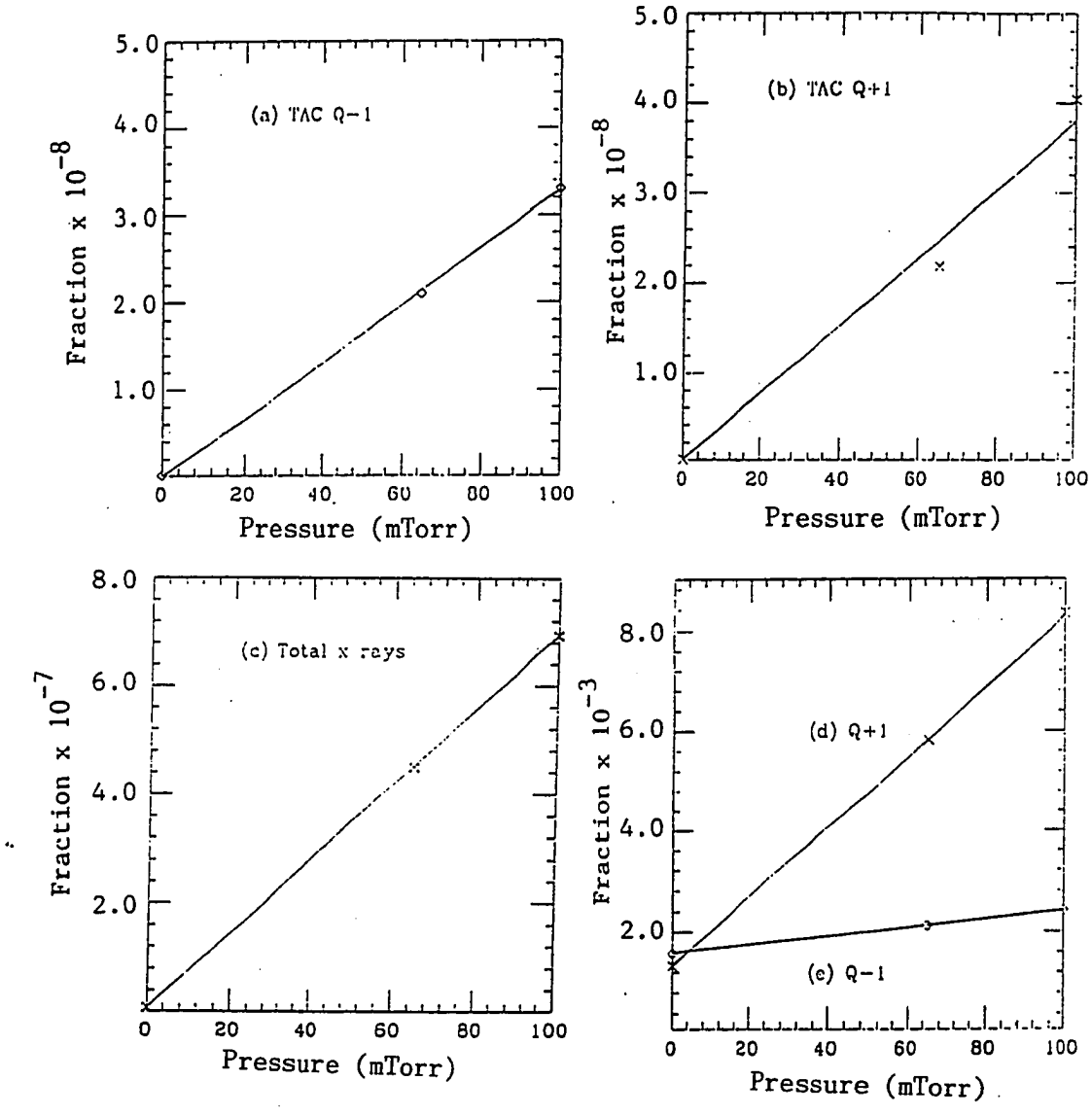

Figure 11. Plots of Various Fractions as a Function of Pressure at 43.3 MeV.

The lines are least squares fit to the data.

shows the typical dependence of the fractions as a function of the target gas-cell pressure at an incident energy of 43.3 MeV. Q+1 represents single-electron loss (or ionization of the projectile ion), Q-1 represents single-electron capture, Total x rays is the total K-shell x-ray yield, TAC Q+1 are the x rays coincident with single- electron loss, and TAC Q-1 represents x rays coincident with single-electron capture. The linearity of the measured fractions versus gas pressure shown in Figure 11 indicated that single collision conditions prevailed within the gas cell. The slopes of such graphs were used to obtain cross sections as described in the next section.

The absolute uncertainty in the charge exchange (capture and loss) cross sections is estimated to be 25-30%. This arises primarily from the uncertainties in the effective target length. An additional significant uncertainty in the charge exchange cross sections could result from changes in the intensity of scattering from beam apertures during a set of measurements. Relative uncertainties are primarily due to counting statistics which were usually determined from the error in fitting a straight line to the experimental fraction versus pressure data.

The total x-ray cross sections and the coincident cross sections have an estimated absolute uncertainty of ±

25%. In this case the uncertainty arises mostly from the uncertainty in the correction for absorption of the x rays in the detector Be window and the dead layers in the silicon crystal in the detector. Relative uncertainties are due to counting statistics.

Determination of Cross-Sections

The fraction of events of type i, F_i, can be defined as the ratio of the number of that type of event, I_i, to the total number of incident particles, I_o

$$F_i = \frac{I_i}{I_o}. \qquad (3.1)$$

The fraction of F_i depends directly on the following: the cross section for the particular type of event (σ_i), the efficiency of the detector (ϵ), the solid angle subtended by the detector ($\Delta\Omega$), and the thickness of the target cell (T) in atoms/cm^2.

Hence F_i can be written as

$$F_i = \frac{I_i}{I_o} = \sigma_i \epsilon \frac{\Delta\Omega}{4\pi} T. \qquad (3.2)$$

The thickness of the target gas cell is given by

$$T = N l_{eff} P \qquad (3.3)$$

where N = 3.3 x 10^{13} atoms/cm^3.mTorr, l_{eff} = effective length

of the target gas cell in cm, and P = pressure in mTorr. Equation (3.2) can then be written as

$$F_i = \sigma_i \epsilon \frac{\Delta\Omega}{4\pi} (N\, l_{eff})\, P. \qquad (3.4)$$

Differentiating the above equation with respect to pressure

$$\frac{dF_i}{dP} = \sigma_i . \epsilon . \frac{\Delta\Omega}{4\pi} (N\, l_{eff}). \qquad (3.5)$$

The left hand side dF_i/dP is the slope of the plot of the fraction of the particular type of events versus pressure. Therefore σ_i, the cross section for that type of event, can be written as

$$\sigma_i = \left(\frac{4\pi}{\epsilon \Delta\Omega\, (N\, l_{eff})} \right) \frac{dF_i}{dP}. \qquad (3.6)$$

$$Let \qquad \frac{4\pi}{\epsilon \Delta\Omega N . l_{eff}} = K$$

$$then \qquad \sigma_i = K \left(\frac{dF_i}{dP} \right) cm^2. \qquad (3.7)$$

The experimental cross-sections were obtained by determining dF_i/dP for each fraction of interest from a least-squares straight-line fit to the experimental data points. The slope of this line, along with the constant K, were used to find the cross-section.

For x-ray emission, the value of the constant, K_x, was

numerically calculated from the geometry of the x-ray detector and the target cell using a computer program written by Clark (1989). In the present case, the product $\epsilon\Delta\Omega l_{eff}$ was found to be .07601 cm resulting in a value of K_x = 5.524 x 10^{-12} cm^2 mTorr/atom.

Hence, the total cross section for x-ray production is given by

$$\sigma_{ix}(Q-1) = 5.524x10^{-12}\left(\frac{dF_i}{dP}\right)cm^2. \qquad (3.8)$$

For the capture and loss cross-sections the value of the constant K_p is given by

$$K_p = \frac{1}{N.l_{eff}}$$

since $\Delta\Omega = 4\pi$ and $\epsilon = 1$ for particle detection. Substituting N = 3.3 x 10^{13} atoms/cm^3 mTorr and l_{eff} = 2.46cm, the value of K_p is found to be, K_p = 1.23 x 10^{-14} cm^2 mTorr/atom. Therefore, the capture and loss cross sections were obtained by using the following formula

$$\sigma_{capture(loss)} = 1.23x10^{-14}\left(\frac{dF_i}{dP}\right)_{capture(loss)} cm^2. \quad (3.9)$$

CHAPTER IV

RESULTS AND DISCUSSION

As mentioned in Chapter I, the main motivation for performing this experiment was to investigate RTE for Mg^{9+} + H_2 because measured cross sections for F^{6+} ions colliding with H_2 were found to be about a factor of two smaller than theory (Schulz et al., 1988). Recently, Bernstein et al. (1991), measured RTE cross sections for collisions of 17-36 MeV F^{6+} ions with H_2. This experiment was also carried out at Western Michigan University using the EN tanden Van de Graaff accelerator. Preliminary results (Western Michigan University, Department of Physics, 1989-1990) of this latter experiment indicated cross sections not much larger than those obtained by Schulz et al. (1988). However, some new measurements, along with a reanalysis (Bernstein, 1990) of the earlier F^{6+} data, have resulted in considerably larger experimental cross sections which are now in agreement with RTE theory.

Tables 1 and 2 list all of the measured cross sections as a function of projectile ion energy for Mg^{9+} ions incident on molecular hydrogen targets. In these tables σ_x is the cross section for total K-shell x-ray production,

$\sigma_x(Q-1)$ is the cross section for x-ray production coincident with single-electron capture, $\sigma_x(Q+1)$ is the cross section for x-ray production coincident with single-electron loss, $\sigma(Q-1)$ is the total single-electron-capture cross section, and $\sigma(Q+1)$ is the total single-electron-loss cross section. For the present experiment involving an H_2 target, the capture and loss cross sections were divided by 2 (two) to account for the molecular nature of the target.

Table 1

Measured Total X-ray and Coincident Cross Sections for Mg^{9+} +H_2 Collisions with relative uncertainties.

E	σ_x	$\sigma_x(Q-1)$	$\sigma_x(Q+1)$
MeV	$x10^{-20}cm^2$	$x10^{-21}cm^2$	$x10^{-21}cm^2$
33.0	(2.9 ± 0.2)	(0.17 ± 0.04)	(1.3 ± 0.1)
37.0	(3.0 ± 0.2)	(0.54 ± 0.05)	(2.0 ± 0.1)
39.4	(3.1 ± 0.2)	(0.82 ± 0.06)	(1.9 ± 0.1)
41.0	(2.8 ± 0.2)	(1.17 ± 0.08)	(1.4 ± 0.1)
42.0	(3.8 ± 0.3)	(1.7 ± 0.1)	(2.0 ± 0.1)
43.3	(3.8 ± 0.3)	(2.0 ± 0.1)	(2.2 ± 0.2)
45.0	(3.5 ± 0.3)	(2.0 ± 0.1)	(2.2 ± 0.2)
47.0	(4.3 ± 0.3)	(2.6 ± 0.2)	(2.1 ± 0.2)
49.0	(3.1 ± 0.2)	(2.6 ± 0.2)	(1.6 ± 0.1)
51.2	(4.1 ± 0.9)	(3.4 ± 0.2)	(1.9 ± 0.2)
52.0	(4.0 ± 0.3)	(3.7 ± 0.3)	(1.8 ± 0.1)
54.0	(3.6 ± 0.3)	(3.3 ± 0.2)	(1.8 ± 0.2)
57.0	(4.3 ± 0.3)	(3.7 ± 0.3)	(1.8 ± 0.3)
58.5	(4.2 ± 0.3)	(3.1 ± 0.2)	(2.0 ± 0.2)
60.0	(4.2 ± 0.3)	(2.6 ± 0.2)	(1.9 ± 0.3)

Table 2

Measured Singles Cross Sections for Mg^{9+} + H_2 Collisions with relative uncertainties.

E MeV	$\sigma(Q-1)$ $x10^{-19}cm^2$	$\sigma(Q+1)$ $x10^{-19}cm^2$
33.0	(4.1 ± 0.3)	(8.7 ± 0.6)
37.0	(2.2 ± 0.2)	(8.9 ± 0.6)
39.4	(1.8 ± 0.1)	(8.7 ± 0.6)
41.0	(1.5 ± 0.1)	(8.7 ± 0.6)
42.0	(1.3 ± 0.1)	(8.5 ± 0.6)
43.3	(1.1 ± 0.1)	(8.6 ± 0.6)
45.0	(1.2 ± 0.1)	(7.8 ± 0.6)
47.0	(0.4 ± 0.4)	(8.1 ± 0.6)
49.0	(0.67 ± 0.05)	(8.0 ± 0.6)
51.2	(0.54 ± 0.04)	(7.8 ± 0.5)
52.0	(0.63 ± 0.05)	(7.8 ± 0.5)
54.0	(0.46 ± 0.05)	(7.7 ± 0.5)
57.0	(0.37 ± 0.03)	(7.2 ± 0.5)
58.5	(0.31 ± 0.02)	(7.1 ± 0.5)

Some of the results are also shown in graphical form in Figures 12, 13, 14, 16 and 17 where the cross sections are plotted as a function of the incident projectile ion energy.

Figure 12 shows the measured cross sections for x rays coincident with electron capture for Mg^{9+} + H_2 collisions (33-60 MeV) compared with the RTE theory (solid line) given by Badnell (1990). The highest energy measured, 60 MeV, was limited by the maximum terminal voltage (6 MV) of the accelerator. In Figure 12 the theoretically calculated

(Badnell, 1990) cross sections have been multiplied by 0.92 to facilitate comparison with the experimental cross sections. There is excellent agreement between the theory and the experimental points over the energy range of the measurements (33-60 MeV). The calculated contributions from KLL transitions are smaller than those from KLn (n > L) transitions. However, the calculated maximum is rather asymmetric with a shoulder near 45 MeV at the position of the peak of the KLL contributions. The data show an indication of this shoulder.

Figure 13 shows single electron capture and loss cross sections as a function of incident projectile ion energy. The capture cross sections show the expected decreasing exponential behavior. These cross sections fall off by an order of magnitude over the energy range of interest (33-60 MeV).

The single-electron loss or ionization cross section shown in Figure 13 decreases slowly with increasing projectile ion energy. This behavior is expected because the major contribution to single-electron loss by a lithiumlike projectile is from interactions of the target nucleus with the projectile L-shell electron. In the energy range studied the projectile ion velocity is considerably greater than the velocity of the projectile shell electron. As the projectile energy is increased the

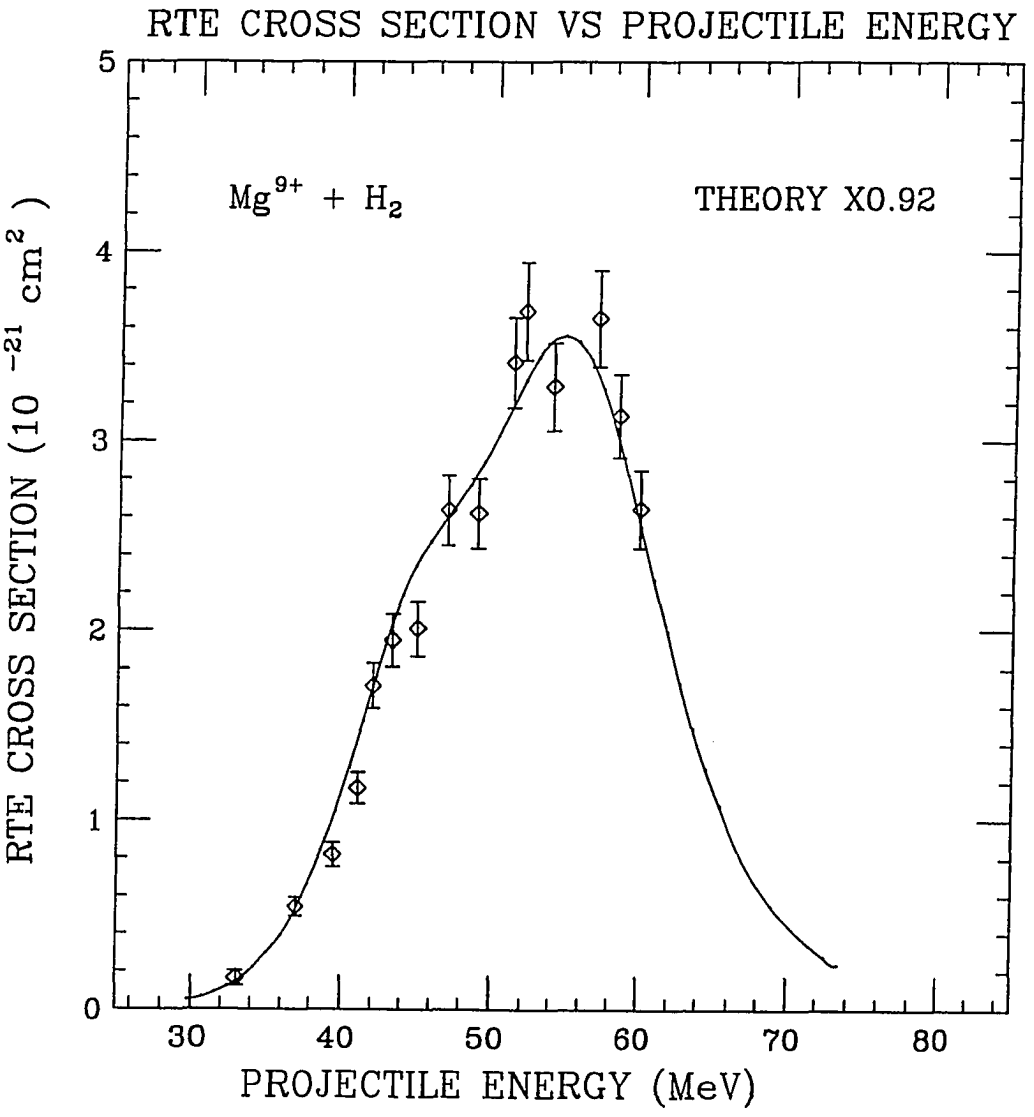

Figure 12. Experimental Cross Sections for Simultaneous Electron Capture and K X-Ray Emission Events as a Function of the Incident Projectile Ion Energy for $Mg^{9+} + H_2$.

The solid curve is the theoretical RTE cross section (Badnell, 1990) multiplied by 0.92.

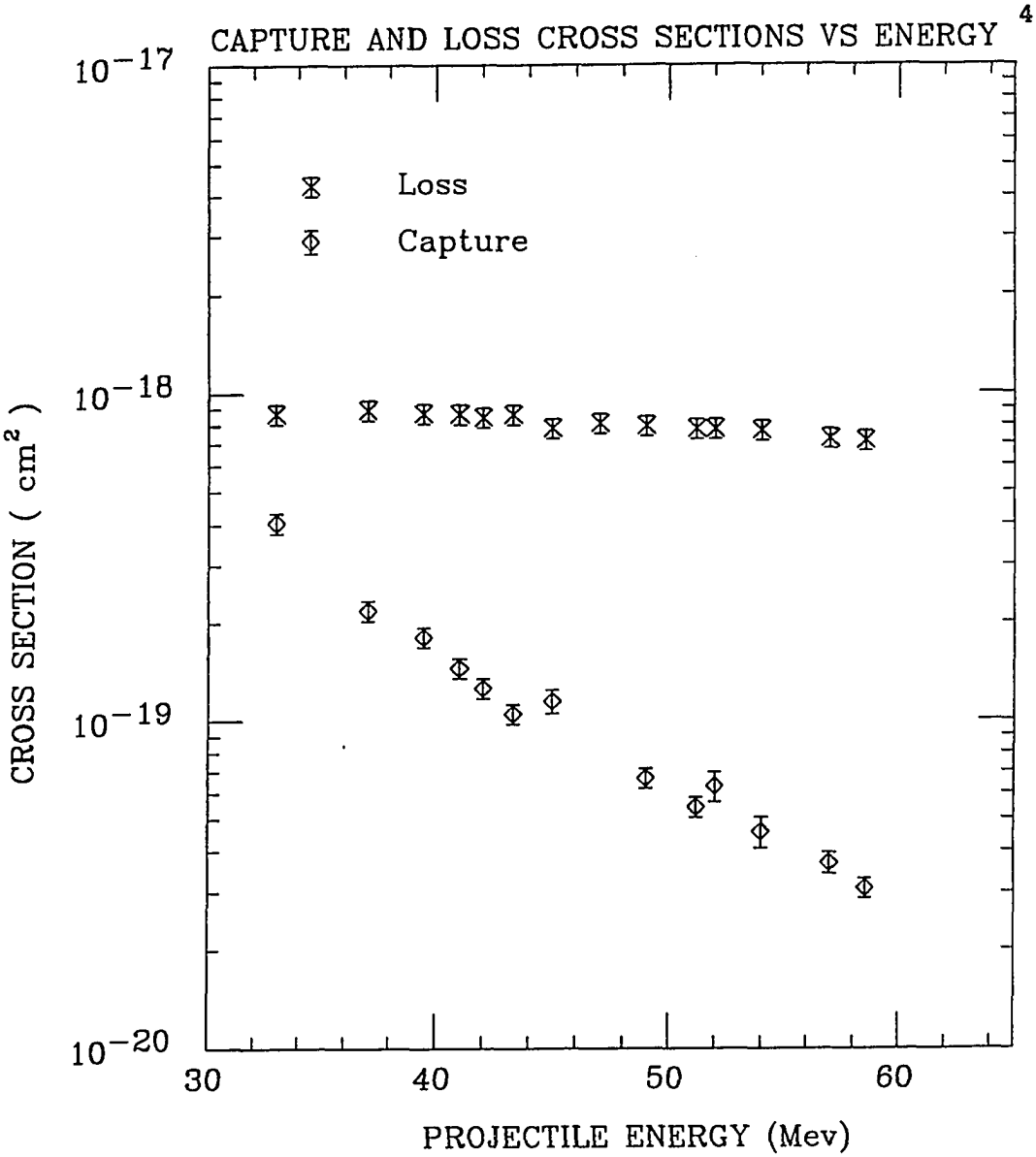

Figure 13. Single Electron Capture and Loss Cross Sections Versus Projectile Ion Energy for $Mg^{9+} + H_2$.

relative velocity increases with a subsequent decrease in the nucleus-electron interaction time resulting in a smaller average momentum transfer which produces a decrease in the cross section.

As shown in Figures 14 and 15 the single electron capture cross sections have the same energy dependence as the empirical single electron-capture scaling rule of Schlachter et al., (1987). However, the absolute values of the experimental cross sections are 35% larger than the prediction of the scaling rule. The reason for this disagreement is not known.

Figure 16 shows cross sections for x-ray production coincident with electron loss, $\sigma_x(Q+1)$, as a function of incident projectile ion energy. It is seen that $\sigma_x(Q+1)$ is essentially independent of energy, within the experimental uncertainty, in the range studied.

Figure 17 shows cross sections for total K-shell x-ray production, σ_x, as a function of incident projectile ion energy. The data for total K-shell x-ray, σ_x, cross sections show a behavior almost similar to $\sigma_x(Q+1)$ data. It is also seen that the cross sections for σ_x are much larger than $\sigma_x(Q+1)$ because the excitation of the electron already present on the projectile contributes strongly to the total K-shell x-ray cross section.

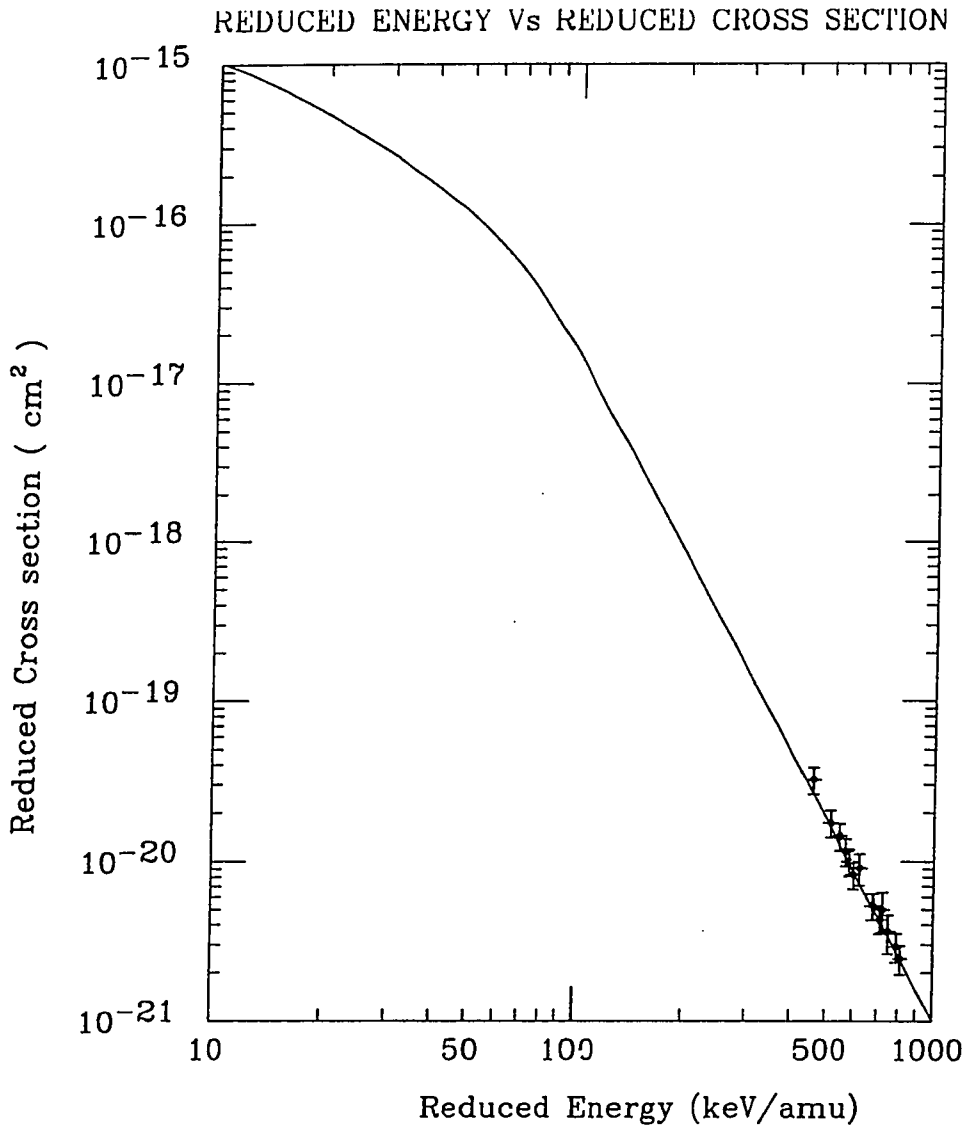

Figure 14. Single Electron Capture Cross Sections for Mg^{9+} + H_2 Compared to the Empirical Scaling Rule of Schlachter et al.(1987).

The graph is drawn using the reduced coordinates defined by equations 2.3 and 2.4.

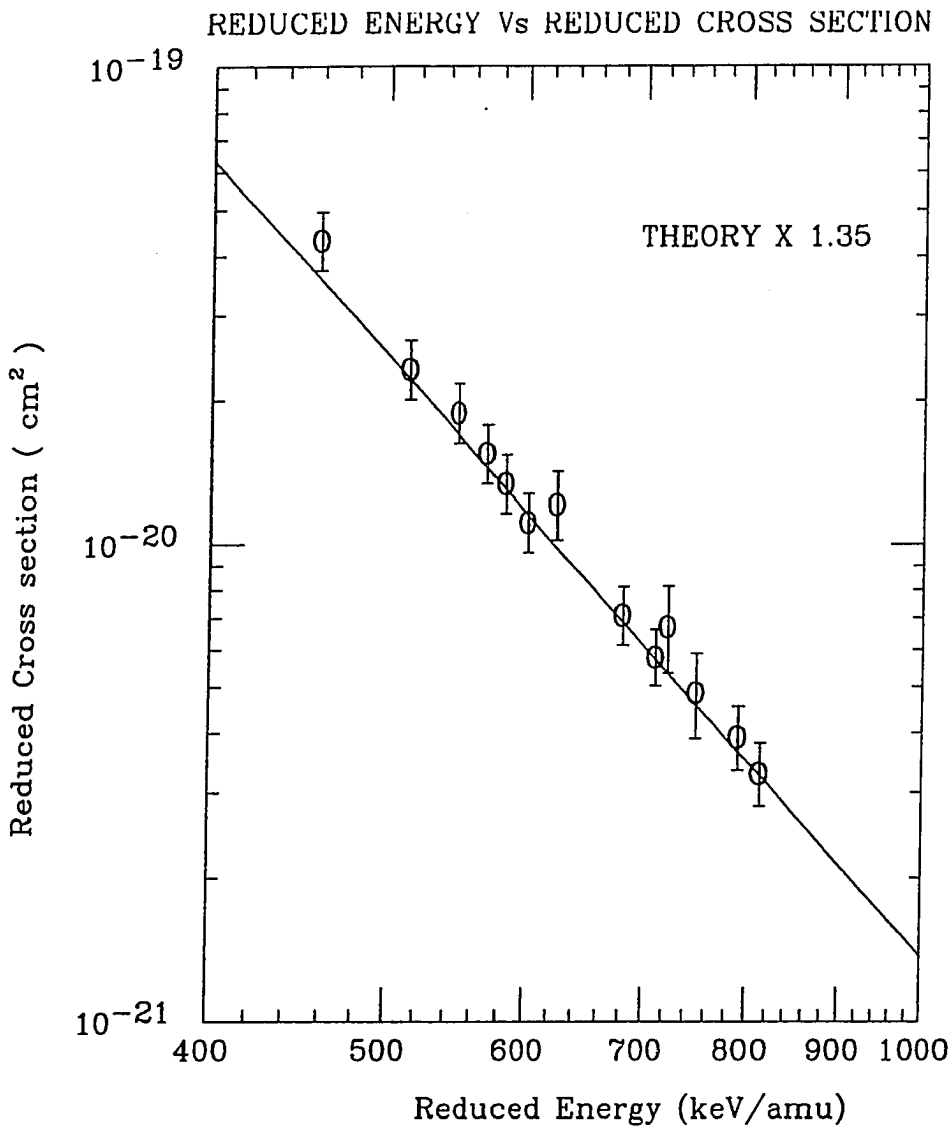

Figure 15. Expanded View of Figure 14 Over the Region of the Measurements.

The calculated curve has been multiplied by 1.35.

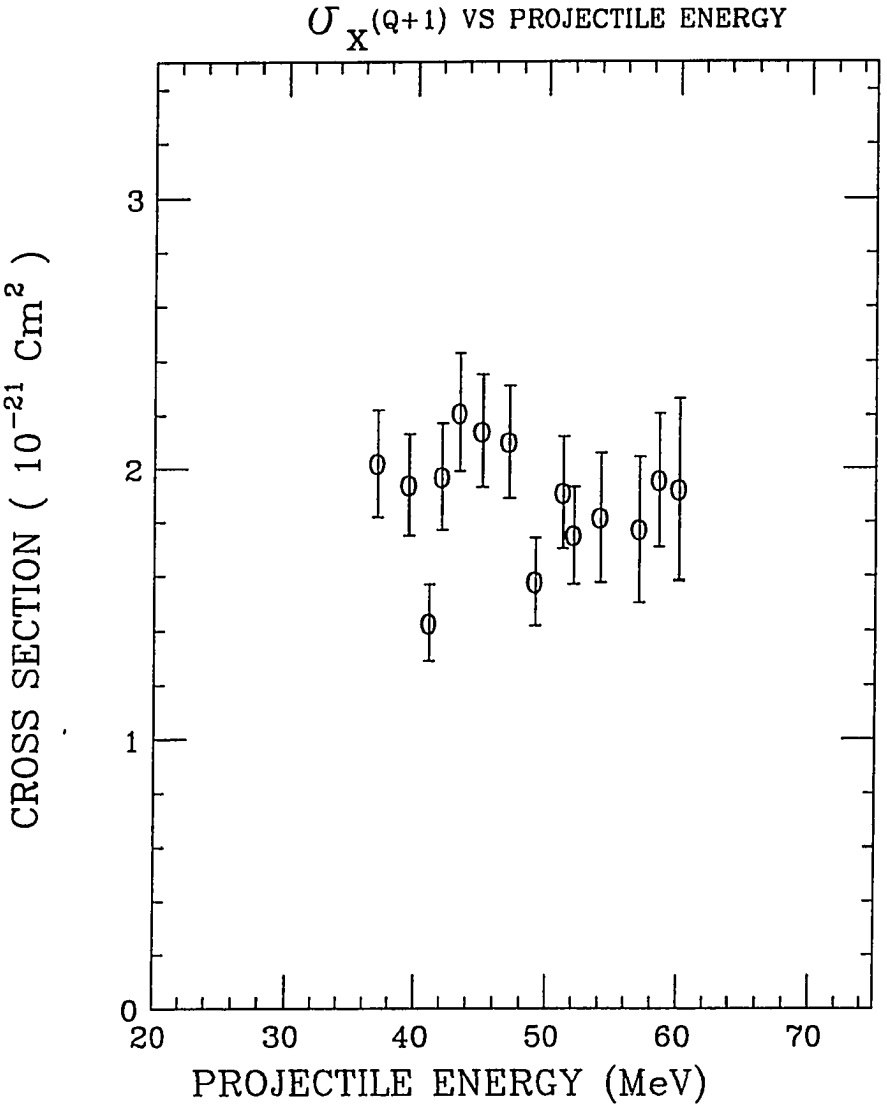

Figure 16. Cross Section for X-Ray Production Coincident With Electron Loss as a Function of Projectile Ion Energy.

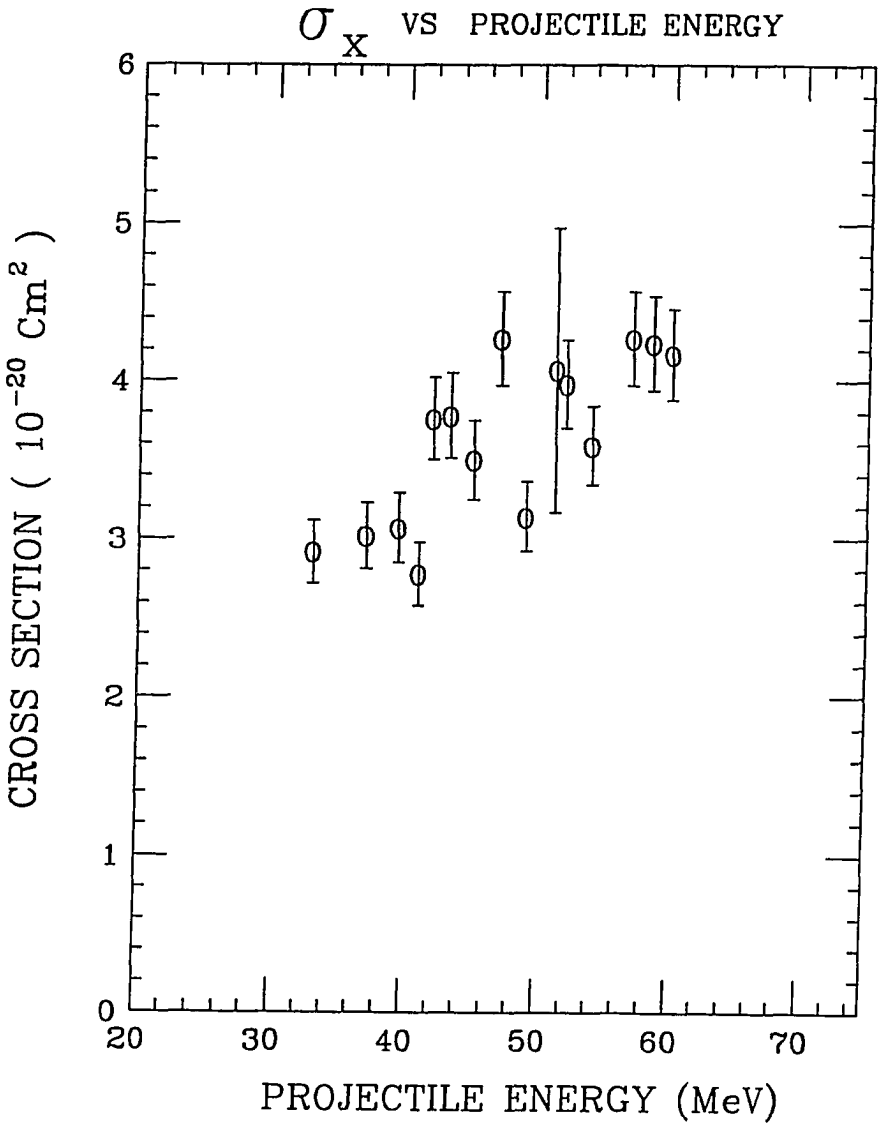

Figure 17. Cross Section for Total K-Shell X-Ray Production as a Function of Projectile Ion Energy.

CHAPTER V

CONCLUSIONS

In the present work resonant transfer and excitation have been investigated for collisions of Mg^{9+} (lithiumlike) projectile ions with a molecular hydrogen gas target. The experimental cross sections for K-shell x rays coincident with electron capture are found to be in good agreement with theoretical RTE calculations (see Figure 12). The theoretical RTE calculations predict that, for the $Mg^{9+} + H_2$ system, the KLL contributions are smaller than the KLn (n >L) contributions. Consequently, the calculated RTE peak has a maximum near 54 MeV, and this peak is rather asymmetric with a shoulder near 45 MeV which results from the KLL resonances. An indication of this shoulder is seen in the experimental data. Thus, the present results confirm the agreement between experiment and theory which has been reported for RTE involving K-shell excitation for projectiles with atomic numbers between 9 and 92 incident on H_2 and He targets.

As discussed in Chapter II, the measurement of RTE cross sections allows one to test calculations of the resonant energies and cross sections for DR for the

projectile ion. It appears that these calculations for Mg^{9+} are correct.

Cross sections for total K-shell x ray production and x rays coincident with electron loss as well as total single-electron-capture and single-electron-loss were measured for $Mg^{9+} + H_2$ collisions as a function of projectile energy in the range from 33 to 60 MeV. The cross sections for K-Shell x-ray production, σ_x, are found to increase somewhat with increasing energy whereas, the cross sections for x-rays coincident with electron loss, $\sigma_x(Q+1)$, is independent of energy within the uncertainties.

It is noted that the single-electron-capture cross sections decrease by an order of magnitude over the energy range of interest. The energy dependence of the single-electron-capture cross sections are found to be in excellent agreement with an empirical scaling rule. However, the absolute values are larger than the predictions of the scaling rule by about 35%. The reason for this disagreement is not known.

The primary purpose of this experiment was to investigate RTE for lithiumlike Mg. As noted in Chapter III special apertures were used in the gas cell to minimize the difference in the effective target length for x-ray events compared to charge-changing events. Because of these apertures, the effective target length for the charge-

change measurements was not as well defined as in the normal arrangement. Additional measurements with the standard apertures in the gas cell would be worthwhile in order to investigate the observed discrepancy between the absolute values of the experimental capture cross sections compared to the predictions of the scaling rule.

BIBLIOGRAPHY

Ali, R., Bhalla, C.P., Cocke, C.L., & Stockli, M. (1990). Dielectronic recombination on heliumlike argon. Physical Review Letters, 64, 633.

Andersen, L.H., Hvelplund, P., Knudsen, H., & Kvistgaard, P. (1989). State selective dielectronic-recombination measurements for He-like oxygen ions in an electron cooler. Physical Review Letters, 62, 2656.

Badnell, N.R. (1989). Fine-structure effects on resonant transfer excitation cross sections for Li-like-ion collisions with H_2 and He. Physical Review A, 40, 3579-3583.

Badnell, N.R. (1990). Private communication.

Belic, D.S., Dunn, G.H., Morgan, R.J., Mueller, D.W., & Timmer, C. (1983). Dielectronic recombination: A crossed-beams observation and measurement of cross section. Physical Review Letters, 50, 339-342.

Bernstein, E.M. (1990). Private communication.

Bernstein, E.M., Clark, M.W., Tanis, J.A., Berkner, K.H., McDonald, R.J., Schlachter, A.S., Stearns, J.W., Graham, W.G., McFarland, R.H., Morgan, T.J., Mowat, J.R., Mueller, D.W., & Stockli, M.P. (1987). Resonant electron transfer and L-Shell excitation for $_{41}N^{31+}$ and $_{57}La^{40+}$ ions. Journal of Physics B Atomic and Molecular Physics, B20, L505-L510.

Bernstein, E.M., Clark, M.W., Tanis, J.A., Woodland, W.T., Berker, K.H., Schlachter, A.S., Stearns, J.W., BuBois, R.D., Graham, W.G., Morgan, T.J., Mueller, D.W., & Stockli, M.P. (1989). Test of predicted $\Delta n \geq 1$ L-shell dielectronic-recombination cross sections. Physical Review A, 40, 4085-4088.

Bernstein, E.M., Kamal, A., Zaharakis, K.E., Clark, M.W., Tanis, J.A., Ferguson, S.M., & Badnell, N.R. (1991). Resonant transfer excitation in collisions of F^{6+} and Mg^{9+} with H_2. Physical Review A, 44, 4210-4214.

Bhalla, C.P., & Karim, K.R. (1989). Resonant transfer and

excitation in collisions of Li-like F^{6+} and Ca^{17+} with light targets. Physical Review A, 39, 6060-6063.

Biggs, F., Mendelsohn, L.B., & Mann, J.B. (1975). Hartee-Fock Compton profiles for the elements. Atomic Data and Nuclear Data Tables, 16, 201-309.

Bitter, M., Von Goeler, S., Cohen, S., Hill, K.W., Sesnic, S., Tenney, F., Timberlake, J., Safronova, U.I., Vainshtein, L.A., Dubak, J., Loulergue, M., Bely Duban, F., & Steenman-Clark, L. (1984). Dielectronic satellite spectra of hydrogenlike titanium (Tixxii). Physical Review A, 29, 661.

Bohr, N., & Lindhard, G. (1954). Electron capture and loss by heavy ions penetrating through matter. Kongelige Danske Videnskabelige Selskab for Matematik og Fysik Meddelser, 28, No. 7.

Brandt, D. (1983). Resonant transfer and excitation in ion-atom collisions. Physical Review A, 27, 1314-1318.

Burgess, A., (1964). Dielectronic recombination and the temperature of the solar corona. Astrophysical Journal, 139, 776-779.

Burgess, A. (1965). A general formula for the estimation of dielectronic recombination coefficients in low-density plasmas. Astrophysical Journal, 141, 1588-1590.

Clark, M.W. (1989). Private communication.

Dittner, P.F., Datz, S., Miller, P.D., Moak, C.D., Stelson, P.H., Bottcher, C., Dress, W.B., Alton, G.D., & Neskovic, N. (1983). Cross sections for dielectronic recombination of B^{2+} and C^{3+} via 2s → 2p excitation. Physical Review Letters, 51, 31-34.

Drawin, H.W. (1978). Plasma impurities and cooling. Physics Reports, 37, 125.

Hahn, Y., Gau, J.N., Omar, G., & Dube, M.P. (1987). Dielectronic recombination for $Mo^{32+, 31+, 30+}$ with L-shell excitation. Physical Review A, 36, 576.

Hahn, Y., (1982). Reduced matrix equtations with reactive components for direct nuclear interactions. Nuclear Physics A, 389, 1-17.

Kilgus, G., Berger, J., Blatt, P., Grieser, M., Habs, D., Hochadel, B., Jaeschke, E., Dramer, D., Neumann, R., Neureither, G., Ott, W., Schwalm, D., Steck, M.,

Stokstad, R., Szmola, E., Wolf, A., Schuch, R., Muller, A., & Wagner, M. (1990). Dielectronic recombination of hydrogenlike oxygen in a heavy-ion storage ring. Physical Review Letters, 64, 737.

Knapp, D.A., Marrs, R.E., Levine, M.A., Bennett, C.L., Chen, M.H., Henderson, J.R., Schneider, M.B., & Scofield, J.H. (1989). Dielectronic recombination of heliumlike nickel. Physical Review Letters, 62, 2104.

Knudsen, H., Haugen, H.K., & Hvelpund, P. (1981). Singl e-electron-capture cross section for medium and high-velocity, highly charged ions colliding with atoms. Physical Review A, 23 597-610.

LaGattuta, K., & Hahn, Y. (1983). Dielectronic recombination rates for Ar^{14+}. Physical Review A, 27, 1675-1677.

McLaughlin, D.J., & Hahn, Y. (1982). Dielectronic recombination cross sections for Si^{11+} and S^{13+}. Physical Review A, 88A, 394-397.

Mitchell, J.B.A., Ng, C.T., Forand, J.L., Levac, D.P., Mitchell, R.E., Sen, A., Miko, D.B., & McGowan, J.Wm. (1983). Dielectronic Recombination Cross Section Measurements for C^{+} ions. Physical Review Letters, 50, 335.

Nasser, I., & Hahn, Y. (1983). Dielectronic recombination rates for heliumlike ions. Journal of Quantum Spectroscopy and Radiation Transfer, 29, 1-8.

Oglesby, C. S. (1985). Resonant electron transfer and K-shell excitation of lithiumlike projectiles in collisions with neutral gas targets. Unpublished Master's thesis, Western Michigan University, Kalamazoo, MI.

Pepmiller, P.L. (1983). Formation of doubly excited two electron ions during F^{8+} + He, Ne or Ar Collisions. Dissertation Abstracts International, 44, 1490B. (University Microfilms No. 83-21, 117)

Pepmiller, P.L., Richard, P., Newcomb, J., Hall, J., & Dillingham, T.R. (1985). Formation of doubly excited two-electron ions during F^{8+} + He, F^{8+} + Ne, F^{8+} + Ar Collisions. Physical Review A, 31, 734.

Richard, P. (1975). Atomic inner-shell processes. Academic, New York, 1, 74-152.

Schlachter, A.S., Stearns, J.W., Berkner, K.H., Stockli,

M.P., Graham, W.G., Bernstein, E.M., Clark, M.W., & Tanis, J.A. (1987). Abstracts of Contributed Papers. In J. Gedes, H.B. Gilbody, A.E. Kingston, C.J. Latimer, & H.J.R. Walters (Eds.), Proceedings of the Fifteenth International Conference of the Physics of Electronic and Atomic Collisions (p. 505). Belfast: Queens University.

Schlachter, A.S., Stearns, J.W., Graham, W.G., Berkner, K.H., Pyle, R.V., & Tanis, J.A. (1983). Electron capture for fast highly charged ions in gas targets: An empirical scaling rule. Physical Review A, 27, 3372-3374.

Schnopper, H.W., Betz, H.D., Hans, D., Delvaille, J.P., Kalata, K., Sohvol, A.R., Jones, K.W., & Wegner, H.E. (1972). Evidence for radiative electron capture by fast, highly stripped heavy ions. Physical Review Letters, 29, 898.

Schulz, M., Schuch, R., Datz, S., Justiniano, E. L. B., Miller, P.D., & Schone, H. (1988). Resonant transfer and excitation in Li-like F colliding with H_2. Physical Review A, 38, 5454-5457.

Seaton, M.J., & Storey, P.J. (1976). Dielectronic recombination. In P.G. Burke & B.L. Moiseiwitsch (Eds.), Atomic processes and applications (pp.133-197). New York: North Holland Publishing.

Steigman, G. (1975). Charge transfer reactions in multiply charged ion-atom collisions. Astrophysical Journal, 199, 642.

Tanis, J.A. (1987). Electron transfer and projectile excitation in single collisions. Nuclear Instruments and Methods in Physics Research A, 262, 52-61.

Tanis, J.A. (1990a). Resonant recombination in ion-atom collisions. In D. Berenyi & G. Hock, Lecture Notes in Physics 376: High-Energy Ion-Atom Collisions (pp.97-111). Berlin: Springer-Verlag.

Tanis, J.A. (1990b). Transfer excitation in ion-atom collisions. In T.A. Carlson, M.O. Krause, & S.T. Manson (Eds.), AIP Conference Proceedings 215: X-Ray and Inner-shell Process (pp. 359-374). New York: American Institute of Physics.

Tanis, J.A., Bernstein, E.M., Clark, M.W., Graham, W.G., McFarland, R.H., Morgan, T.J., Johnson, B.M., Jones, K.W., & Meron, M. (1985). Evidence for uncorrelated

electron capture and K-shell excitation in S^{13+} + He collisions. Physical Review A, 31, 4040-4042.

Tanis, J.A., Shafroth, S.M, Willis, J.E., Clark, M., Swenson, J., Strait, E.M., & Mowat, J.R. (1981). Simultaneous electron capture and excitation in S + Ar collisions. Physical Review Letters,47, 828-831.

Western Michigan University, Department of Physics. (1989-90). Research Report. Kalamazoo: Author.

Whitten, B.L., Hazi, A.U., Chen, M.H., & Hagelstein, P.L. (1986). Effect of dielectronic recombination on the kinetics of neonlike selenium. Physical Review A, 33, 2171.